Biaxial extensional viscous dissipation in sheets expansion formed by impact of drops of Newtonian and non-Newtonian fluids

Ameur Louhichi [1,2] Carole-Ann Charles,[1] Ty Phou,[1] Dimitris Vlassopoulos [2]
Laurence Ramos [1,*] and Christian Ligoure [1,†]

[1]*Laboratoire Charles Coulomb (L2C), Université de Montpellier, CNRS, Montpellier, France*

[2]*Institute of Electronic Structure and Laser, FORTH, Heraklion 70013, Crete, Greece*
and Department of Materials Science and Technology, University of Crete, Heraklion 70013, Crete, Greece

We investigate freely expanding liquid sheets made of either simple Newtonian fluids or solutions of high molecular water-soluble polymer chains. A sheet is produced by the impact of a drop on a quartz plate covered with a thin layer of liquid nitrogen that suppresses shear viscous dissipation due to an inverse Leidenfrost effect. The sheet expands radially until reaching a maximum diameter and subsequently recedes. Experiments indicate the presence of two expansion regimes: the capillary regime, where the maximum expansion is controlled by surface tension forces and does not depend on the viscosity, and the viscous regime, where the expansion is reduced with increasing viscosity. In the viscous regime, the sheet expansion for polymeric samples is strongly enhanced as compared to that of Newtonian samples with comparable zero-shear viscosity. We show that data for Newtonian and non-Newtonian fluids collapse on a unique master curve where the maximum expansion factor is plotted against the relevant effective *biaxial extensional* Ohnesorge number that depends on fluid density, surface tension, and the biaxial extensional viscosity. For Newtonian fluids, this biaxial extensional viscosity is six times the shear viscosity. By contrast, for the non-Newtonian fluids, a characteristic *Weissenberg number*-dependent biaxial extensional viscosity is identified, which is in quantitative agreement with experimental and theoretical results reported in the literature for biaxial extensional flows of polymeric liquids.

I. INTRODUCTION

Over the last 15 years, the understanding of drop impact on solid targets has progressed considerably due to high-speed imaging methods [1], allowing one to observe in real time the fate of a drop upon impact under various experimental conditions and to probe a rich variety of phenomena, including dynamics of sheets in the expansion and receding regimes, spatiotemporal evolution of the thickness of the sheets [2,3], fingering instabilities [4–6], and fractures and production of satellite droplets [7–9]. Concerning the nature of the impacting drops, mainly Newtonian fluids of different viscosities have been investigated, although a few relevant studies with shear-thickening fluids [10], shear-thinning fluids [11–17], yield stress fluids [18], or Maxwell fluids without shear thinning [19,20]. Most studies have been performed on drops impacting a flat surface that can be smooth or rough [21], horizontal or tilted [22], hydrophobic or hydrophilic [23]. Often, surfaces have a

---

*laurence.ramos@umontpellier.fr
†christian.ligoure@umontpellier.fr

very large size compared to that of the drop such that the entire spreading event occurs on the target [8,14,15,24–27], but targets of size comparable to that of the drops [2,3,16,28,29] or drops impacting only partially a small target [30] have also been studied.

The complex interaction of a drop with a solid surface during drop collision may be removed or at least significantly reduced by using repellent surfaces, which avoid a direct contact between the liquid sheet and the solid target. Repellent surfaces include superhydrophobic surfaces [31], hot plates above the Leidenfrost temperature [32,33] or sublimating surfaces [20,34]. Nevertheless, the fact that shear viscous dissipation can be neglected during the expansion of the sheet after impact does not mean that there is no viscous dissipation process. Indeed, *biaxial extensional* viscous dissipation is dominant in freely expanding sheets. Surprisingly this has never been documented to the best of our knowledge, except in a very recent paper [35], where the authors have attributed an inhibition of a drop-substrate contact during drop impact to a large increase of the extensional viscosity.

A possible reason for ignoring the biaxial extensional viscous dissipation is that for sheets expanding completely on a solid surface, viscous dissipation should be dominated by shear. For small targets however, both shear and biaxial extensional viscous dissipation processes may be relevant: this is the goal of a future publication. In the present paper, only biaxial extensional viscous dissipation is relevant as the sheet expands freely due to the inverse Leidenfrost effect discussed below. In this work, we investigate the expansion dynamics of free sheets of a viscoelastic thinning fluid produced upon impacting a single drop on a repellent surface in inverse Leidenfrost conditions, and compare it to the respective response of Newtonian fluids. We demonstrate that accounting for the viscous dissipation due to biaxial extensional viscosity during the expansion of the sheet is crucially important. We provide a simple approach to evaluate the biaxial extensional viscosity of thinning viscoelastic fluids, and finally propose a model to quantitatively account for the viscosity dependence of the maximum expansion of sheets.

The paper is organized as follows. We first describe the materials and methods. We then show the shear rheological properties of the viscoelastic fluids of interest and their behavior upon impact on a repellent surface. Subsequently, we rationalize the results by accounting for the biaxial extensional viscosity and by means of a simple scaling model. The main conclusions are summarized in the last section.

II. MATERIALS AND METHODS

A. Materials

We investigate solutions of polyethylene-oxide (PEO) of high molecular weight ($M_v = 8000$ kDa) from Sigma-Aldrich. Several samples with concentration C between 10^{-3} wt% and 2 wt% are prepared by adding PEO powder, as received, to the appropriate volume of deionized pure water, or mixtures of water and glycerol (20 wt%, 35 wt%, and 41.66 wt% glycerol), and leave the solution under stirring at $T = 25\,°C$ for 24 h at least in the dark, until complete dissolution. Note that, in order to enhance the visualization contrast, all PEO solutions are colored using a Nigrosin dye (from Sigma-Aldrich) at concentration 0.025 wt%. The surface tension of high molecular weight PEO solutions is independent of polymer concentration ($\gamma = 62$ m Nm^{-1}) [36]. Pendant drop experiments confirm that the addition of dye does not affect the surface tension of the final solutions. In addition, in order to compare the behavior of viscoelastic polymer solutions with that of simple fluids, we use two classes of Newtonian fluids, mixtures of water and glycerol and silicon oils. Silicon oils, with shear viscosities from 5.2 to 1075 mPa s and an average surface tension of 20 mN/m [37], were purchased from Sigma Aldrich and used as received. Mixtures of water and glycerol with concentrations ranging from 22 to 97.5 wt% glycerol are prepared, yielding shear viscosities from 1.7 to 1910 mPa s (depending on the glycerol weight fraction and temperature), densities from 1.05 to 1.25 g/ml, and an average surface tension of 65 mN/m (as measured with a pendant drop setup).
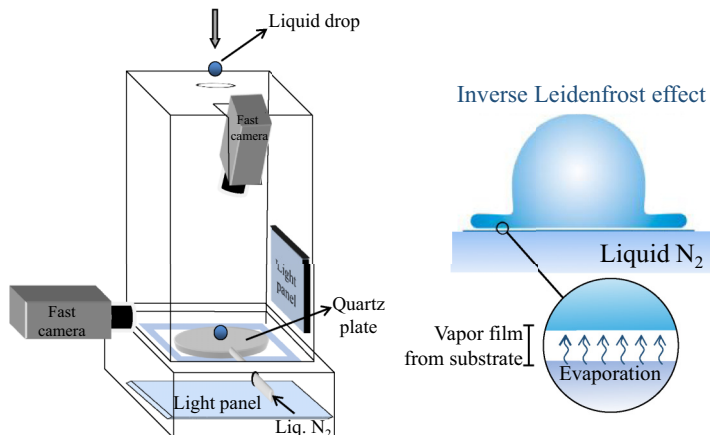
FIG. 1. Left: Schematic illustration of the impact experiments setup showing a drop falling on a liquid nitrogen thin layer. The expansion event is recorded using two fast cameras allowing concomitant top and side visualizations. Right: Adapted from Ref. [34], schematic of the inverse Leidenfrost effect at the origin of the shear free expansion.

B. Methods

1. Drop impact experiments

To substantially eliminate the role of friction or adhesion with the solid surface on the impact dynamics, we work under inverse Leidenfrost conditions. This is achieved by impacting a drop at ambient temperature T (between 18.5 and 22.5 °C) on a polished quartz slide covered with a thin layer of liquid nitrogen (N_2) at $T = -196$ °C (see Fig. 1). The setup is described elsewhere [20]. Upon impact of the drop, a vapor cushion forms at the liquid interface due to the evaporation of N_2, providing a unique scenario of nonwetting slip conditions that eliminates shear viscous dissipation [34,38]. The rare cases where the impacting drop comes in direct contact with the surface with instantaneous freezing are eliminated, so the nitrogen vapor film keeps the liquid drop separated from the surface for all the reported experiments. Before each impact, the quartz slide is first cleaned by blowing N_2 gas, and then a thin layer (typical thickness 50 nm as measured by ellipsometry) of liquid N_2 is deposited on the slide. The liquid is injected from a syringe pump with a flow rate of 1 ml/min through a needle placed above the target, from the side as shown in Fig. 1. The diameter of the falling drop is constant, $d_0 = 3.9 \pm 0.2$ mm, as measured by image analysis and confirmed from the drop mass. The drop falls from a height $h = 91$ cm, yielding an impact velocity $v_0 = \sqrt{2gh} = 4.2$ ms^{-1} (g is the acceleration of gravity). The drop impact is recorded from the top [Fig. 2(a)] using a high-speed camera (Phantom V 7:3) operated at 6700 frames/s with a resolution of 800×600 pixels^2. The angle between the camera axis and the horizontal plane is fixed to about 10°. A second high-speed camera (Phantom miro M310), operated at 3200 frames/s with a resolution of 1280×800 pixels^2, is eventually used simultaneously to record a side view [Fig. 2(b)].

2. Image analysis

The time evolution of the sheet size is measured with ImageJ software by analyzing top-view images. We first subtract the background image from the expansion movie and highlight the rim by a binary thresholding. This allows us to determine the sheets contour and measure its area A. Note that A does not include the fingers emanating from the rim of the expanding film; they may appear for low viscous samples (Fig. 2) but do not develop for more viscous ones (see Fig. 4 below). An apparent sheet diameter is simply deduced: $d = \sqrt{\frac{4A}{\pi}}$. The results are obtained by averaging for each sample the time evolution of the sheet diameter from three different experiments. Note, however,
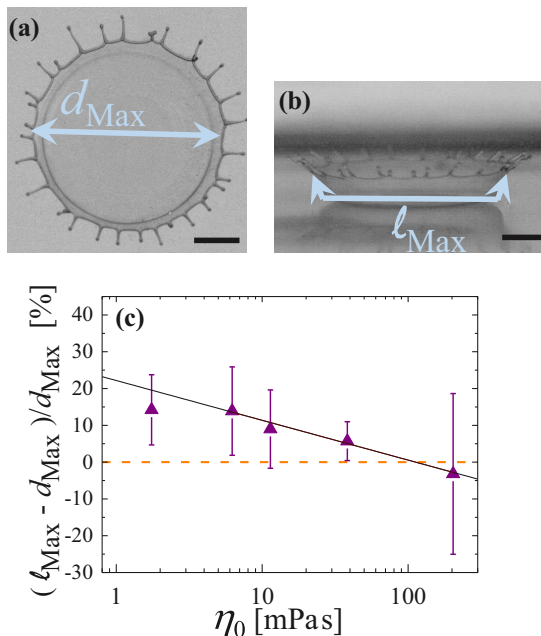
FIG. 2. (a) Top-view and (b) side-view snapshots of the maximum expansion of a low viscous Newtonian sample (22wt% glycerol-water mixture), revealing that the effective diameter d_{Max} from the top view underestimates the maximum expansion of the sheet ℓ_{Max}. (c) Relative side-view correction effect (in %) as a function of shear viscosity of Newtonian glycerol-water. The line is an empirical fit of the data points (symbols).

that corrections have to be performed for low-viscosity samples. Indeed, side-view images reveal the occurrence of a so-called corona splash [Fig. 2(b)] [8], for low viscous Newtonian samples. This implies that the routine standard analysis using top-view images would underestimate the maximum expansion diameter. The side view allows one to evaluate the actual diameter of the sheet [see ℓ_{Max} in Fig. 2(b)]. The fractional underestimation, defined as $\frac{\ell_{\text{Max}} - d_{\text{Max}}}{d_{\text{Max}}}$, with d_{Max} the maximum diameter measured from top-view images, is plotted as a function of the samples zero-shear viscosity, η_0, in Fig. 2(c). We find that the fractional underestimation decreases logarithmically with η_0, from about 22wt% for the lowest viscosity sample and vanishes for $\eta_0 \geqslant 100$ mPa s. Hence, in the following, quantitative corrections are made for the maximum expansion diameter based on the empirical logarithmic law. For samples with a shear viscosity larger than 100 mPa, the sheet remains flat and no correction is needed.

3. Rheology

Linear viscoelastic and steady shear viscosity measurements are performed with a MCR302 stress-controlled rheometer (Anton Paar, Austria), operating in the strain-control mode and equipped with a stainless steel cone and plate geometry with a diameter of 50 mm, cone angle of 1° and truncation of 101 μm. Temperature control ($\pm 0.2\,°$C) is achieved by means of a Peltier element. The linear viscoelastic spectra are obtained by applying a small amplitude sinusoidal strain, such that data are obtained in the linear regime ($\gamma = 10\%$), varying the angular frequency, ω, from 100 to 0.01 rad/s, and measuring the storage, $G'(\omega)$, and loss, $G''(\omega)$, moduli. The complex viscosity is calculated from the linear viscoelastic spectra as $|\eta^\star(\omega)| = \frac{\sqrt{[G'^2(\omega) + G''^2(\omega)]}}{\omega}$. The steady shear viscosity, $\eta(\dot{\gamma})$ is measured by applying a ramp of steady shear rate varying from 0.01 to 1000 s^{-1}.
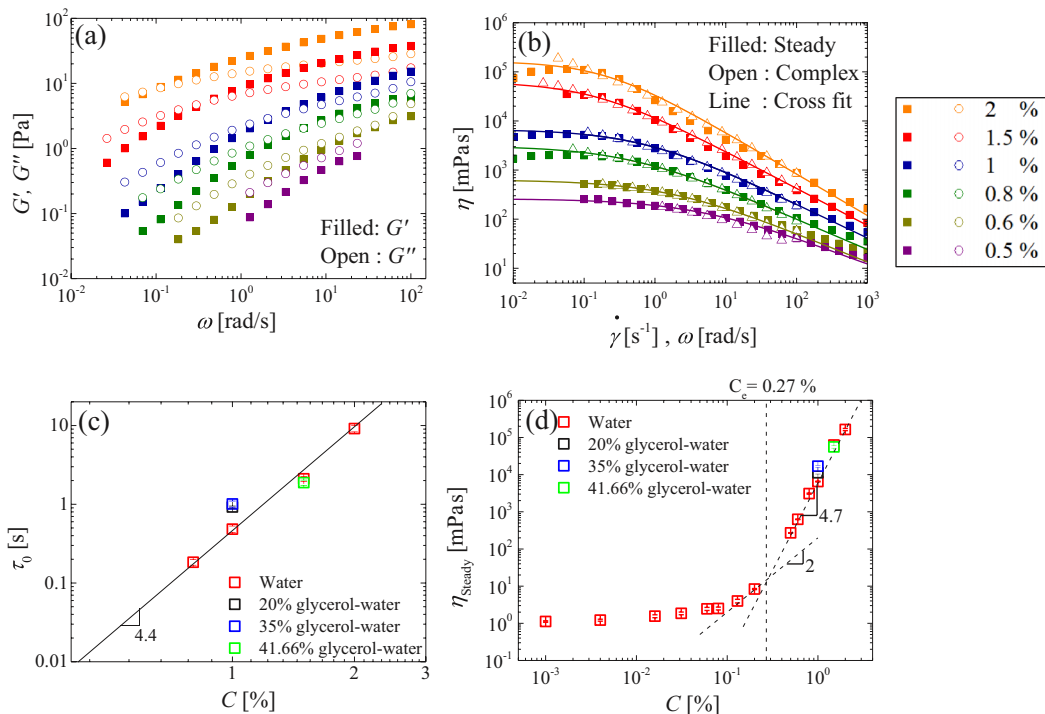
FIG. 3. (a) Frequency dependence of the storage (G') and loss (G'') moduli, and (b) complex viscosity as a function of frequency (open symbols) and steady shear viscosity as a function of shear rate (filled samples), and fits (lines) using the Cross equation [Eq. (1)], for samples with different PEO concentrations C as indicated in the legend. (c) Evolution with C of the terminal relaxation time and (d) of the zero shear viscosity.

III. RESULTS

A. Shear rheology

Figure 3(a) shows the dynamic moduli as a function of oscillatory frequency for aqueous polymer solutions with various concentrations. For $C > 0.6\,\mathrm{wt\%}$, the crossover of G' and G'' marks a characteristic relaxation time τ_0, which is the best estimate for the onset of the terminal regime. Figure 3(c) shows that $\tau_0 \sim C^{0.44}$ s. This scaling exponent is in the range that have been reported for high molecular weight PEO aqueous solutions [39]. Results for samples prepared with mixtures of water and glycerol are consistent with those obtained for pure water samples [Fig. 3(c)].

The zero shear viscosity, η_0, varies by more than 5 orders of magnitude from 1 to 10^5 mPa s for the samples investigated. The variation of η_0 with polymer concentration, C, reveals the two expected regimes [Fig. 3(d)]: an unentangled regime for $C < 0.27\%$, where the viscosity increases slowly with the polymer concentration, and an entangled regime at larger concentration, where $\eta_0 \propto C^{4.7}$, in agreement with predictions by scaling arguments based on the tube model [40].

Figure 3(b) depicts the complex viscosity, $|\eta^\star(\omega)|$ as a function of frequency, along with the steady shear viscosity, $\eta(\dot{\gamma})$ as a function of shear rate, $\dot{\gamma}$. The nice collapse of the dynamic and steady data validates the Cox-Merz rule [41]. We find that all samples are strongly shear thinning and that an empirical fit by means of the Cross model provides a good description of the shear-thinning behavior of PEO solutions [continuous lines in Fig. 3(b)] [42]:

$$\eta_s(\dot{\gamma}) = \eta_\infty + \frac{\eta_0 - \eta_\infty}{1 + (k\dot{\gamma})^n}. \tag{1}$$

(a)

(b)
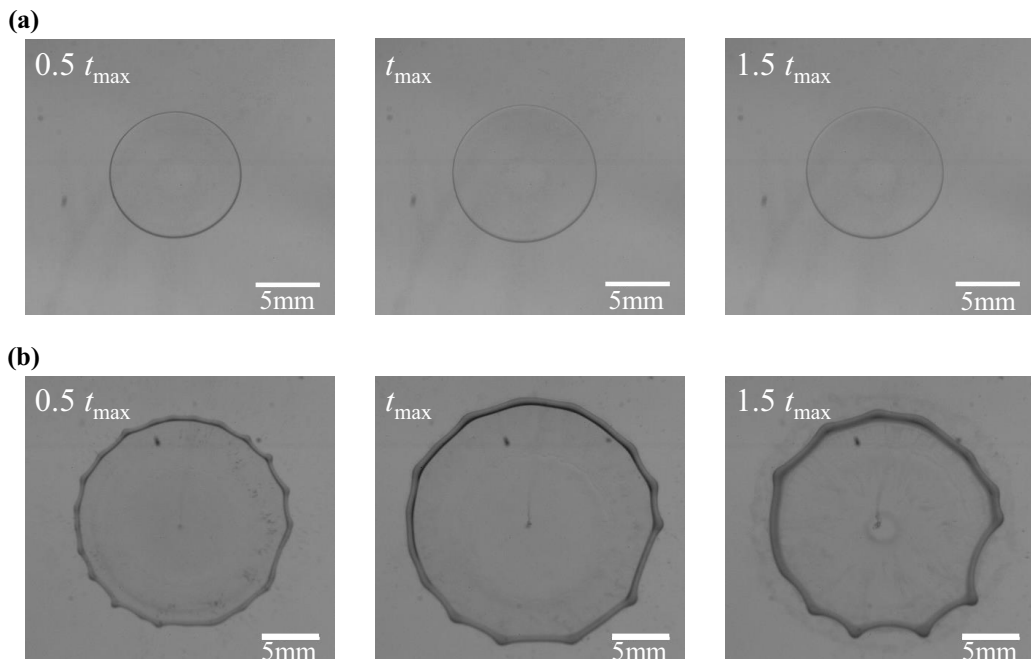
FIG. 4. Snapshots taken at different times, as indicated, during the expansion and retraction of the sheet for (a) a Newtonian silicon oil with shear viscosity $\eta_0 = 658$ mPa s; maximum expansion reached at time $t_{max} = 5.22$ ms and (b) a PEO solution with $C = 0.6$wt% and $\eta_0 = 628$ mPa s; maximum expansion reached at time $t_{max} = 5.02$ ms. The bar sets the scale.

Here η_∞ is the viscosity at very large shear rate that we set equal to the solvent viscosity (water or water-glycerol mixture), η_0 is the zero-shear viscosity [plotted in Fig. 3(d)], n is the shear-thinning exponent, and the parameter k is the inverse of a critical shear rate that delimitates a Newtonian regime from a shear-thinning regime. We find that the shear-thinning exponent n increases with increasing C from 0.59 to 0.85. Moreover, for all concentrations the fitting parameter k is monotonically increasing with C, similarly to the characteristic relaxation time τ_0, and it marks the onset of shear thinning.

B. Drop impact experiments

Once hitting the repellent surface, the drop expands freely in air until reaching a maximum expansion. It then retracts because of surface tension. This corresponds to an an axisymmetric biaxial extensional flow. The overall behavior is illustrated in Fig. 4, which depicts snapshots of the drop after its impact for a PEO solution with $C = 0.6$% ($\eta_0 = 628$ mPa s) and for a Newtonian sample of comparable zero-shear viscosity ($\eta_0 = 658$ mPa s). The two samples display strikingly different behavior: the viscoelastic fluid drop expands much more than the Newtonian drop and moreover forms a thicker rim. More quantitatively, we show [Figs. 5(a) and 5(b)] selective raw data for the time evolution of the effective sheet diameter normalized by the original drop, $\frac{d}{d_0}$, for PEO solutions at different concentrations and Newtonian liquids (here silicon oils, but water-glycerol mixtures exhibit the same behavior) with different viscosities. The origin of time is chosen at the time when the drop hits the liquid nitrogen layer. Expansion and retraction regimes are shown, yielding a bell shape for the curves. We note that the curves for the viscoelastic fluids are very symmetric as opposed to the ones for the more viscous Newtonian fluids, where a very long
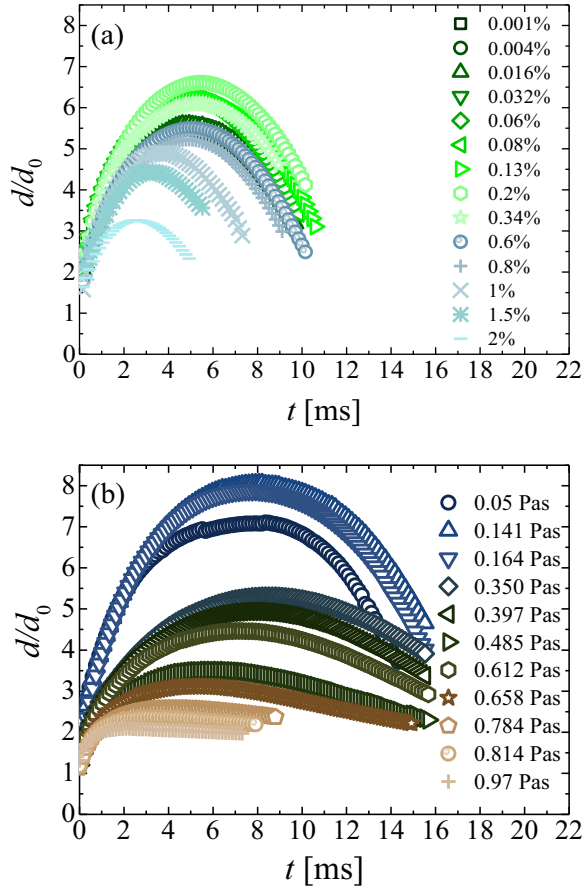
FIG. 5. Time evolution of the sheet diameter normalized by the initial drop diameter for (a) PEO solutions with different concentrations and (b) silicon oils with different shear viscosities, as indicated in the legends. The origin of the time is taken at the drop impact.

retraction regime is measured. These findings deserve deeper investigations in the future, but in the following, we focus on the maximum expansion diameter d_{Max}.

For a biaxial extensional flow, during the expansion of free liquid sheets after impact on a repellent surface, the relevant viscosity is the biaxial extensional viscosity defined as $\eta_{\mathrm{B}} = \frac{\sigma_{rr} - \sigma_{zz}}{\dot{\epsilon}}$, where $\dot{\epsilon}$ is the strain rate, and σ_{rr} and σ_{zz} are the stress tensor components in cylindrical coordinates.

For a Newtonian fluid the constant biaxial extensional viscosity $\eta_{\mathrm{B}} = \eta_{\mathrm{B}}^0 = 6\eta_0$, where η_0 is the zero-shear viscosity and 6 is the Trouton ratio [43]. As a first-order analysis aiming at rationalizing the expansion dynamics of sheets of Newtonian and thinning fluids, we consider the maximum expansion factor, d_{Max}/d_0, with d_0 the initial drop diameter and plot [Fig. 6(a)] this quantity as a function of the biaxial extensional viscosity η_{B}^0. Note that the shear viscosity is measured at the room temperature of the impact experiment; this is of particular importance for water-glycerol mixtures which exhibit a strong temperature dependant viscosity [44]. Similarly to findings for Newtonian fluids impacting a small solid target [19], two regimes are observed for both polymer solutions and Newtonian fluids. At low η_{B}^0 a capillary regime prevails, where the maximum expansion is mainly driven by a balance between surface tension forces and inertial forces, with viscous dissipation being negligible. Hence, this regime is characterized by a plateau. By contrast, in the viscous regime at higher η_{B}^0, d_{Max} decreases monotonically with increasing viscosity.
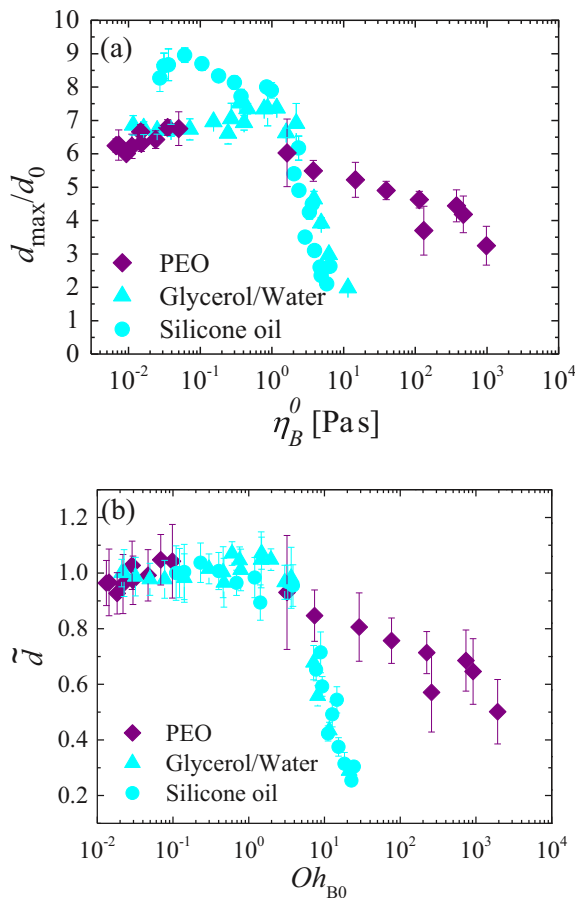
FIG. 6. (a) Maximum diameter of the sheet normalized by the initial drop diameter as a function of the biaxial extensional viscosity, and (b) normalized maximum expansion factor as a function of the biaxial extensional Ohnesorge number, for PEO solutions and for Newtonian liquids.

To get further insight into the observed behavior, we use the normalized maximum expansion factor, $\tilde{d}$, adopting the same definition as in Refs. [12,19]:

$$\tilde{d} = \frac{d_{\mathrm{Max}}}{d_{\mathrm{Max}}^{\mathrm{cap}}}, \tag{2}$$

where $d_{\mathrm{Max}}^{\mathrm{cap}}$ is the maximum expansion diameter in the capillary regime (at low viscosity). This normalized quantity allows us to compare drops with different initial sizes and different surface tensions. In addition, to account for different surface tensions for different samples, data are plotted against the biaxial extensional Ohnesorge number, [Oh_{B0}], the ratio of biaxial extensional viscous forces to inertial and surface tension forces:

$$\mathrm{Oh}_{\mathrm{B0}} = \frac{\eta_{\mathrm{B}}^{0}}{\sqrt{\rho \gamma d_0}} \tag{3}$$

with ρ the sample density and γ the surface tension. Figure 6(b) shows the evolution of $\tilde{d}$ with Oh_{B0} for both polymer solutions and Newtonian fluids. The data for the two types of Newtonian samples overlap nicely onto a master curve and exhibit a capillary regime (for $\mathrm{Oh}_{\mathrm{B0}} \lesssim \mathrm{Oh}_{\mathrm{B0}}^{c} = 2$) characterized by a plateau, followed by a biaxial extensional viscous dissipation regime. We find
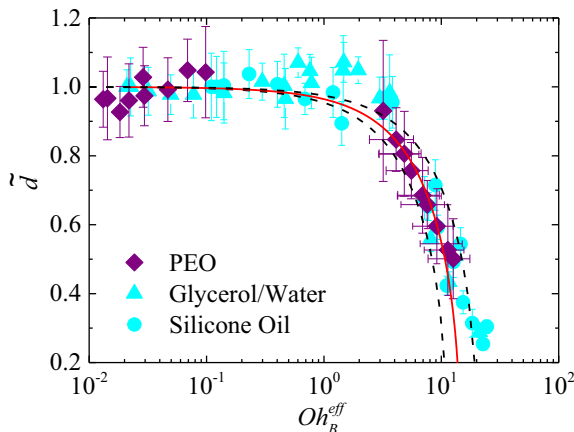
FIG. 7. Normalized maximum expansion factor as a function of the effective biaxial extensional Ohnesorge number for polymer solutions and for the two classes of Newtonian samples. The thin continuous line is the best fit with Eq. (11), and the dashed lines are used to evaluate error bars on the fit parameter.

that for the thinning fluids, the onset of the viscous regime takes place at approximatively the same critical biaxial extensional Ohnesorge number Oh_{B0}^c as for Newtonian liquids. Interestingly, however, $\tilde{d}$ decreases much more gradually with Oh_{B0} as compared to Newtonian fluids in the viscous regime. This clearly suggests the importance of a biaxial extensional thinning of the polymer solutions in the viscous dissipation regime. In the next section, we provide a rationalization for the biaxial extensional expansion dynamics of sheets produced with Newtonian and non-Newtonian fluids.

IV. DISCUSSION

A. Rationalization of biaxial extensional thinning

From the data of Fig. 6(b), one can easily define an effective biaxial extensional thinning viscosity η_B^{shift} for polymer samples belonging to the viscous regime ($Oh_{B0} > Oh_{B0}^c$) by shifting horizontally the experimental data point so that they fall on the master curve found for Newtonian samples. The shifted values are discussed in Fig. 9 below. No shift is performed in the capillary regime ($Oh_{B0} < Oh_{B0}^c$) since viscous dissipation is not relevant. Doing so we build a master curve (Fig. 7) for the maximum expansion $\tilde{d}$ as a function of Oh_B^{Thin} for all types of samples, where the effective biaxial extensional Ohnesorge number $Oh_B^{Thin} = Oh_{B0}$ for Newtonian samples and viscoelastic thinning samples in the capillary regime and $Oh_B^{Thin} = \frac{\eta_B^{shift}}{\eta_B^0}Oh_{B0}$ for visoelastic thinning samples in the viscous regime. Below we rationalize the shifting of Fig. 7 and the use of biaxial extensional viscosity of non-Newtonian fluids.

1. Determination of the pertinent strain rate

Experimentally, measuring properly the biaxial extensional viscosity is a challenging task, especially for relatively low viscosity fluids such as the present polymers [45–51]. In order to rationalize η_B^{shift}, the first step is to properly account for the deformation rate experienced by sheets during their expansion in air. Here we provide an estimate.

The effective strain rate, defined as $\dot{\varepsilon} = \frac{1}{d}\frac{\partial d}{\partial t}$, is not constant in the expansion regime, but decreases with time and vanishes at maximum expansion (Fig. 8). Note that the film expansion is a time-dependent problem, but here we focus on the maximum diameter (end of expansion process) and measure the average rate experienced by the sheet during the expansion. The average value for
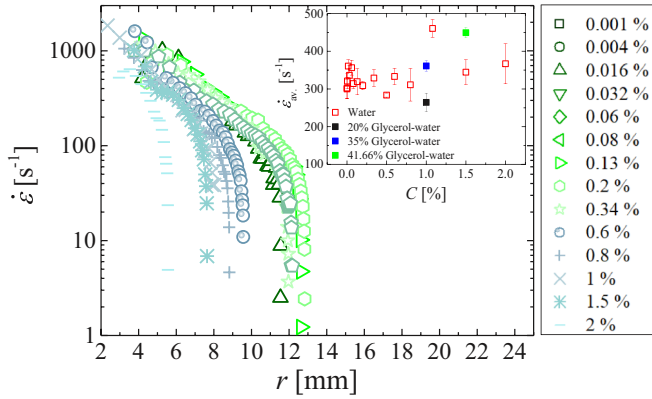
FIG. 8. Evolution of the expansion strain rate as a function of the sheet radius during its expansion for aqueous PEO solutions at different concentrations, as indicated in the legend. Inset: Average strain rate calculated according to Eq. (4) as a function of concentration. Error bars represent the standard deviation from three different experiments.

the strain rate in the expansion regime is then calculated as

$$\dot{\varepsilon}_{\text{av}} = \frac{\int_0^{r_{\text{Max}}} r \dot{\varepsilon}\, dr}{\int_0^{r_{\text{Max}}} r\, dr}. \tag{4}$$

Here $r_{\text{Max}} = \frac{d_{\text{Max}}}{2}$ is te radius of the sheet at its maximum expansion. We get an average strain rate for each solutions that it is used for the rest of the analysis. Note, however, that within experimental errors ($\simeq 15\%$ as shown in the inset of Fig. 8), the effective strain rate does not vary significantly with concentration. Indeed, we obtain a value of $338 \pm 49\ \text{s}^{-1}$ by averaging over all samples, including the PEO solutions prepared in glycerol-water mixtures.

2. Biaxial extensional viscosity

Given the difficulty in obtaining reliable experimental data for the biaxial extensional viscosity $\eta_B(\dot{\varepsilon})$ with our samples, we attempt at providing reasonable estimations To this end, we rely on two pioneering experimental works for the measurements of the biaxial extensional viscosity of viscoelastic solutions [52,53], where similar scaling have been found in spite of using different techniques and different samples: wormlike micelles in Ref. [52] and concentrated polymer solutions in Ref. [53]. At low Weissenberg numbers (Wi $= \dot{\varepsilon}\tau_0 < 1$), i.e., for rates lower than the inverse of the terminal relaxation time, τ_0, the biaxial extensional viscosity is independent of the rate and follows the expectation for a Newtonian fluid: $\eta_B = \eta_B^0 = 6\eta_0$ with η_0 the zero-shear viscosity. By contrast, when Wi > 1, the biaxial extensional viscosity decreases with rate, $\eta_B \sim \dot{\varepsilon}^{-p}$ with a thinning exponent $p = 0.5$ [53]. This scaling has been also predicted by Marrucci and Ianniruberto [54] using a tube-based model for polymer melts hence, pointing out the universality of the biaxial extensional thinning behavior.

Based on the similar linear viscoelastic response for the PEO solutions and those investigated in Refs. [52,53], we expect our samples to exhibit a similar behavior for the biaxial extensional viscosity as a function of expansion rate. Thus, for each impact experiment in the viscous regime, we define an effective Weissenberg number as Wi$^{\text{eff}} = \tau_0 \dot{\varepsilon}_{\text{av}}$, where τ_0 is given by linear shear rheology measurements for the data showing crossover between G' and G'' and extrapolated, according to the power law presented in Fig. 3(c), for data without the crossover (0.5wt% and 0.6wt%); $\dot{\varepsilon}_{\text{av}}$ is measured from experiments [Fig. 8(b)]. The effective biaxial extensional thinning is characterized by the experimental data points (Wi$^{\text{eff}}$, η_B^{shift}), where η_B^{shift} are obtained from Fig. 7. We show in Fig. 9
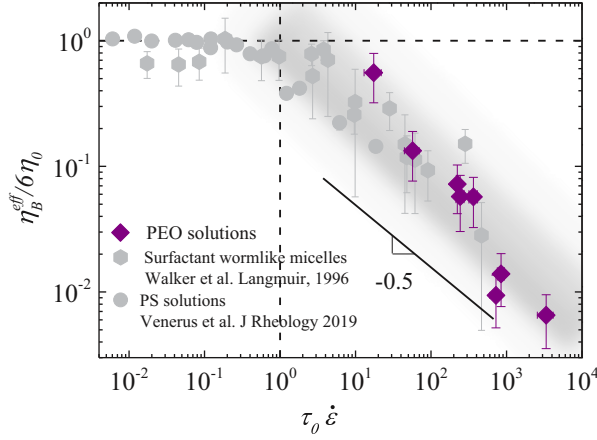
FIG. 9. Effective biaxial extensional viscosity of PEO solutions, extracted from the manual shift of the data in Fig. 7, normalized by the plateau biaxial extensional viscosity as a function of the Weissenberg number, plotted together with literature data as indicated in the legend. A unique master biaxial extensional flow curve is obtained with a thinning exponent of -0.5 in agreement with theoretical predictions (see text). The gray zone highlights the -0.5 slope.

the variation of the normalized effective biaxial extensional viscosity of PEO solutions $\eta_{\text{B}}^{\text{shift}}/(6\eta_0)$ as a function of the effective Weissenberg number Wi^{eff} obtained from drop impact experiments in the viscous regime. On the same plot, we report the experimental data of Refs. [52,53]. We find a remarkable agreement between our shifted values and those from the literature, even though the expansion sheet dynamics that result from the impact of drops are nonstationary, supporting our simple approach.

B. Rationalization of the maximal expansion by considering the biaxial deformation

To go one step further, we provide below scaling laws to account semiquantitatively for the dependence of the maximum expansion on the biaxial extensional viscosity (Fig. 7). We restrict our analysis to Newtonian samples. Indeed, for the normalized maximum expansion factor, each non-Newtonian sample in the viscous regime can be replaced by a Newtonian sample exhibiting the same normalized maximum expansion factor a shown before.

We adopt an energy conservation balance and first consider the capillary regime, for which the initial kinetic energy is assumed to be fully converted into surface energy at the maximum expansion of the sheet:

$$\tfrac{1}{2}mv_0^2 \simeq 2\pi\gamma\left(d_{\text{Max}}^{\text{cap}}\right)^2, \tag{5}$$

where $m = \rho\pi d_0^3/6$ is the mass of the drop and $d_{\text{Max}}^{\text{cap}}$ is the diameter at maximum expansion of the sheet in the capillary regime where viscous dissipation is negligible. In the viscous regime, we need to add to the right-hand side of Eq. (5) a term accounting for the viscous dissipation, which here is assumed to result only from the biaxial extensional deformation:

$$\tfrac{1}{2}mv_0^2 \simeq 2\pi\gamma d_{\text{Max}}^2 + E_{\text{B}}. \tag{6}$$

Combining Eqs. (5) and (6), we obtain for the normalized maximum expansion factor, $\tilde{d}$,

$$\tilde{d} = \frac{d_{\text{Max}}}{d_{\text{Max}}^{\text{cap}}} = \sqrt{1 - \frac{2E_{\text{B}}}{mv_0^2}}, \tag{7}$$

with E_B the biaxial extensional extensional energy dissipated during the process of sheet expansion. To a first approximation, E_B can be written as

$$E_B \approx \int_0^{t_{\text{Max}}} dt \int_V \sigma_B(\dot{\varepsilon})\dot{\varepsilon}\, dV, \tag{8}$$

where $V = \frac{\pi d_0^3}{6}$ is the volume of the drop, $\sigma_B(\dot{\varepsilon}) = \eta_B \dot{\varepsilon}$, and t_{Max} is the time to reach maximum expansion. Hence, assuming also a volume conservation with a uniform thickness sheet, Eq. (8) can be rewritten as

$$E_B \approx \eta_B \frac{\pi d_0^3}{6} \int_0^{t_{\text{Max}}} \left(\frac{1}{d} \frac{\partial d}{\partial t} \right)^2 dt. \tag{9}$$

Using a simple first-order scaling approach to calculate the strain rate, we consider $\frac{\partial d}{\partial t} \approx \frac{d_{\text{Max}} - d_0}{t_{\text{Max}}}$ and a geometric average between the initial and final values of the sheet diameter, $d \approx \sqrt{d_0 d_{\text{Max}}}$, Eq. (9) reads

$$E_B \approx \eta_B \frac{\pi d_0^2}{6} \frac{(d_{\text{Max}} - d_0)^2}{d_{\text{Max}} t_{\text{Max}}}. \tag{10}$$

Here $\frac{(d_{\text{Max}} - d_0)^2}{d_{\text{Max}} t_{\text{Max}}}$ can be considered as an apparent velocity, v_{app}, close to the initial expansion speed of the drop upon impact. Combining Eqs. (7) and (10) together with the definition of the biaxial extensional Ohnesorge number, one predicts

$$\tilde{d} = \sqrt{1 - \alpha \text{Oh}_B} \tag{11}$$

with $\alpha = \frac{2 v_L v_{\text{app}}}{v_0^2}$ and $v_L = \sqrt{\frac{\gamma}{\rho d_0}}$ is the typical velocity of free oscillations of the drop [55]. We find that the functional form of Eq. (11) reproduces very nicely the experimental data (Fig. 7), which implies that v_{app} is approximatively constant. The best fit of the data (continuous red line) yields, for all concentrations, $\alpha = 0.06 \pm 0.02$, where the error bars are used to obtain the two envelopes of the data (dashed black lines). This value is compared to the theoretical expectations for the parameter α. For Newtonian fluids, $v_{\text{app}} = 2.3 \pm 1.2$ m/s, thus $\alpha = 00.25 \pm 0.02$, Overall, the fit parameter of the master curve is thus found in reasonable agreement with the ones calculated using the different experimental quantities, thus justifying the relevance of our approach.

V. CONCLUSION

Drop impact experiments on repellent surfaces have been performed with Newtonian fluids and shear-thinning polymer solutions. Two regimes for the maximum expansion diameter of freely expanding sheets have been identified: a capillary regime, where the maximum expansion does not depend on viscosity, and a viscous regime, where the maximum expansion is reduced with increasing viscosity. We have demonstrated that the dominant source of viscous dissipation is the biaxial extensional deformation during sheet expansion, which consequently controls the maximum expansion of the sheets in the viscous regime. We have provided a scaling prediction of the sheet maximum expansion as a function of the biaxial extensional Ohnesorge number, in good quantitative agreement with our experimental results. For viscoelastic thinning fluids, we have proposed a simple approach to measure the biaxial extensional thinning viscosity based on the maximum expansion factor of a freely expanding sheet: the relevant characteristic thinning viscosity is simply given by the viscosity of a Newtonian fluid with the same normalized expansion factor; it obeys the behavior of the biaxial extensional viscosity of polymeric samples as a function of the Weissenberg number in stationary conditions, providing one considers the mean biaxial extensional rate of the sheet during the expansion regime, as the relevant strain rate for the Weissenberg number. Our approach constitutes a first and crucial step toward the development of a new class of biaxial extensional

rheometry tools based on drop impact experiments but needs further investigations (in current progress) including drops of different diameters and different impact heights.

[1] S. T. Thoroddsen, T. G. Etoh, and K. Takehara, High-speed imaging of drops and bubbles, Annu. Rev. Fluid Mech. **40**, 257 (2008).

[2] C. Vernay, L. Ramos, and C. Ligoure, Free radially expanding liquid sheet in air: Time- and space-resolved measurement of the thickness field, J. Fluid Mech. **764**, 428 (2015).

[3] Y. Wang and L. Bourouiba, Drop impact on small surfaces: Thickness and velocity profiles of the expanding sheet in the air, J. Fluid Mech. **814**, 510 (2017).

[4] S. S. Yoon, R. A. Jepsen, M. R. Nissen, and T. J. O'Hern, Experimental investigation on splashing and nonlinear fingerlike instability of large water drops, J. Fluids Struct. **23**, 101 (2007).

[5] T. S. T and J. Sakakibara, Evolution of the fingering pattern of an impacting drop, Phys. Fluids **10**, 1359 (1998).

[6] H. Marmanis and S. T. Thoroddsen, Scaling of the fingering pattern of an impacting drop, Phys. Fluids **8**, 1344 (1996).

[7] D. van der Meer, Impact on granular beds, Annu. Rev. Fluid Mech. **49**, 463 (2017).

[8] C. Josserand and S. T. Thoroddsen, Drop impact on a solid surface, Annu. Rev. Fluid Mech. **48**, 365 (2016).

[9] D. Bonn, J. Eggers, J. Indekeu, J. Meunier, and E. Rolley, Wetting and spreading, Rev. Mod. Phys. **81**, 739 (2009).

[10] F. Boyer, E. Sandoval-Nava, J. H. Snoeijer, J. F. Dijksman, and D. Lohse, Drop impact of shear thickening liquids, Phys. Rev. Fluids **1**, 013901 (2016).

[11] N. Laan, K. G. de Bruin, D. Bartolo, C. Josserand, and D. Bonn, Maximum Diameter of Impacting Liquid Droplets, Phys. Rev. Appl. **2**, 863 (2014).

[12] S. M. An and S. Y. Lee, Maximum spreading of a shear-thinning liquid drop impacting on dry solid surfaces, Exp. Thermal Fluid Sci. **38**, 140 (2012).

[13] J. J. Cooper-White, R. C. Crooks, and D. V. Boger, A drop impact study of worm-like viscoelastic surfactant solutions, Colloids Surf. A **210**, 105 (2002).

[14] R. Crooks and D. V. Boger, Influence of fluid elasticity on drops impacting on dry surfaces, J. Rheol. **44**, 973 (2000).

[15] D. Izbassarov and M. Muradoglu, Effects of viscoelasticity on drop impact and spreading on a solid surface, Phys. Rev. Fluids **1**, 023302 (2016).

[16] A. Rozhkov, B. Prunet-Foch, and M. Vignes-Adler, Dynamics and disintegration of drops of polymeric liquids, J. Non-Newtonian Fluid Mech. **134**, 44 (2006).

[17] H. K. Huh, S. Jung, K. W. Seo, and S. J. Lee, Role of polymer concentration and molecular weight on the rebounding behaviors of polymer solution droplet impacting on hydrophobic surfaces, Microfluid. Nanofluid., **18**, 1221 (2015).

[18] L,-H, Luu and Y. Forterre, Drop impact of yield-stress fluids, J. Fluid Mech. **632**, 301 (2009).

[19] S. Arora, C. Ligoure, and L. Ramos, Interplay between viscosity and elasticity in freely expanding liquid sheets, Phys. Rev. Fluids **1**, 083302 (2016).

[20] S. Arora, J. M. Fromental, S. Mora, T. Y. Phou, L. Ramos, and C. Ligoure, Impact of Beads and Drops on a Repellent Solid Surface: A Unified Description, Phys. Rev. Lett. **120**, 148003 (2018).

[21] R. Rioboo, M. Marengo, and C. Tropea, Time evolution of liquid drop impact onto solid, dry surfaces, Exp. Fluids **33**, 112 (2002).

[22] A. L. N. Moreira, A. S. Moita, E. Cossali, M. Marengo, and M. Santini, Secondary atomization of water and isooctane drops impinging on tilted heated surfaces, Exp. Fluids **43**, 297 (2007).

[23] M. Lee, Y. S. Chang, and H.-Y. Kim, Drop impact on microwetting patterned surfaces, Phys. Fluids **22**, 072101 (2010).

[24] G. German and V. Bertola, Impact of shear-thinning and yield-stress drops on solid substrates, J. Phys.: Condens. Matter **21**, 375111 (2009).

[25] J. B. Lee, D. Derome, R. Guyer, and J. Carmeliet, Modeling the maximum spreading of liquid droplets impacting wetting and nonwetting surfaces, Langmuir **32**, 1299 (2016).

[26] C. Ukiwe and D. Y. Kwok, On the maximum spreading diameter of impacting droplets on well-prepared solid surfaces, Langmuir **21**, 666 (2005).

[27] D. C. D. Roux and J. J. Cooper-White, Dynamics of water spreading on a glass surface, J. Colloid Interface Sci. **277**, 424 (2004).

[28] A. Rozhkov, B. Prunet-Foch, and M. Vignes-Adler, Dynamics of a liquid lamella resulting from the impact of a water drop on a small target, Proc. R. Soc. London **460**, 2681 (2004).

[29] E. Villermaux and B. Bossa, Drop fragmentation on impact, J. Fluid Mech. **668**, 412 (2011).

[30] S. Lejeune, T. Gilet, and L. Bourouiba, Edge effect: Liquid sheet and droplets formed by drop impact close to an edge, Phys. Rev. Fluids **3**, 083601 (2018).

[31] D. Richard, C. Clanet, and D. Quéré, Surface phenomena: Contact time of a bouncing drop, Nature (London) **417**, 811 (2002).

[32] L. H. J. Wachters, L. Smulders, J. R. Vermeulen, and H. C. Kleiweg, The heat transfer from a hot wall to impinging mist droplets in the spheroidal state, Chem. Eng. Sci. **21**, 1231 (1966).

[33] A.-L. Biance, C. Clanet, and D. Quéré, Leidenfrost drops, Phys. Fluids **15**, 1632 (2003).

[34] C. Antonini, I. Bernagozzi, S. Jung, D. Poulikakos, and M. Marengo, Water Drops Dancing on Ice: How Sublimation Leads to Drop Rebound, Phys. Rev. Lett. **111**, 014501 (2013).

[35] M. Y. Pack, A. Yang, A. Perazzo, B. Qin, and H. A. Stone, Role of extensional rheology on droplet bouncing, Phys. Rev. Fluids **4**, 123603 (2019).

[36] B. H. Cao and M. W. Kim, Molecular weight dependence of the surface tension of aqueous poly(ethylene oxide) solutions, Faraday Discuss. **98**, 245 (1994).

[37] A. Crisp, E. de Juan Jr., and J. Tiedeman, Effect of silicone oil viscosity on emulsification, Arch. Ophtalmol. **105**, 546 (1987).

[38] S. Chen and V. Bertola, The impact of viscoplastic drops on a heated surface in the Leidenfrost regime, Soft Matter **12**, 7624 (2016).

[39] M. Ortiz, D. De Kee, and P. J. Carreau, Rheology of concentrated polyethylene oxide solutions, J. Rheol. **38**, 519 (1994).

[40] M. Rubinstein and R. H. Colby, *Polymer Physics* (Oxford University Press, Oxford, 2003).

[41] W. P. Cox and E. H. Merz, Correlation of dynamic and steady flow viscosities, J. Polym. Sci. **28**, 619 (1958).

[42] M. M. Cross, Rheology of non-Newtonian fluids: A new flow equation for pseudoplastic systems, J. Colloid Sci. **30**, 417 (1965).

[43] C. W. Macosko, *Rheology: Principles, Measurements and Applications* (Wiley-VCH, New York, 1994).

[44] J. B. Segur and H. E. Oberstar, Viscosity of glycerol and its aqueous solutions, Ind. Eng. Chem. **43**, 2117 (1951).

[45] J. M. Maerker and W. R. Schowalter, Biaxial extension of an elastic liquid, Rheologica Acta **13**, 627 (1974).

[46] D. D. Joye and G. W. Poehlein, A bubble inflation technique for the measurement of viscoelastic properties in equal biaxial extensional flow, Trans. Soc. Rheol. **16**, 421 (1972).

[47] D. C. Venerus, T. Y. Shiu, T. Kashyap, and J. Hosttetler, Continuous lubricated squeezing flow: A novel technique for equibiaxial elongational viscosity measurements on polymer melts, J. Rheol. **54**, 1083 (2010).

[48] M. Johnson, N. Murphy, R. Ekins, J. Hanley, and S. Jerrams, Equi-biaxial fatigue testing of EPM utilising bubble inflation, Polymer Testing **53**, 122 (2016).

[49] H. M. Huang and J. L. Kokini, Measurement of biaxial extensional viscosity of wheat-flour doughs, J. Rheol. **37**, 879 (1993).

[50] P. Hachmann and J. Meissner, Rheometer for equibiaxial and planar elongations of polymer melts, J. Rheol. **47**, 989 (2003).

[51] C. A. Cathey and G. G. Fuller, Uniaxial and biaxial extensional viscosity measurements of dilute and semi-dilute solutions of rigid rod polymers, J. Non-Newtonian Fluid Mech. **30**, 303 (1988).

[52] L. M. Walker, P. Moldenaers, and J. F. Berret, Macroscopic response of wormlike micelles to elongational flow, Langmuir **12**, 6309 (1996).

[53] D. C. Venerus, R. M. Mick, and T. Kashyap, Equibiaxial elongational rheology of entangled polystyrene melts, J. Rheol. **63**, 157 (2019).

[54] G. Marrucci and G. Ianniruberto, Interchain pressure effect in extensional flows of entangled polymer melts, Macromolecules **37**, 3934 (2004).

[55] F. R. S Rayleigh, On the capillary phenomena of jets, Proc. R. Soc. London **29**, 71 (1879).